Collaborative Large-Scale Dense 3D Reconstruction with Online Inter-Agent Pose Optimisation

Stuart Golodetz* Tommaso Cavallari* Nicholas A. Lord* Victor A. Prisacariu David W. Murray Philip H. S. Torr

Department of Engineering Science, University of Oxford

{smg,tommaso,nicklord,victor,dwm,phst}@robots.ox.ac.uk

Abstract

Reconstructing dense, volumetric models of real-world 3D scenes is important for many tasks, but capturing large scenes can take significant time, and the risk of transient changes to the scene goes up as the capture time increases. These are good reasons to want instead to capture several smaller sub-scenes that can be joined to make the whole scene. Achieving this has traditionally been difficult: joining sub-scenes that may never have been viewed from the same angle requires a high-quality relocaliser that can cope with novel poses, and tracking drift in each sub-scene can prevent them from being joined to make a consistent overall scene. Recent advances in mobile hardware, however, have significantly improved our ability to capture medium-sized sub-scenes with little to no tracking drift. Moreover, highquality regression forest-based relocalisers have recently been made more practical by the introduction of a method to allow them to be trained and used online. In this paper, we leverage these advances to present what to our knowledge is the first system to allow multiple users to collaborate interactively to reconstruct dense, voxel-based models of whole buildings. Using our system, an entire house or lab can be captured and reconstructed in under half an hour using only consumer-grade hardware.

1. Introduction

Reconstructing dense, volumetric models of real-world 3D scenes is an important task in computer vision and robotics, with applications in content creation for films, games and augmented reality [23], cultural heritage preservation [48] and building information modelling [32]. Since the seminal KinectFusion work of Newcombe et al. [33], which demonstrated real-time voxel-based reconstruction of a desk-sized scene in real time using only a consumer-grade RGB-D sensor, huge progress has been made in increasing the size of scene we are able to reconstruct [34, 36, 37] and in com-

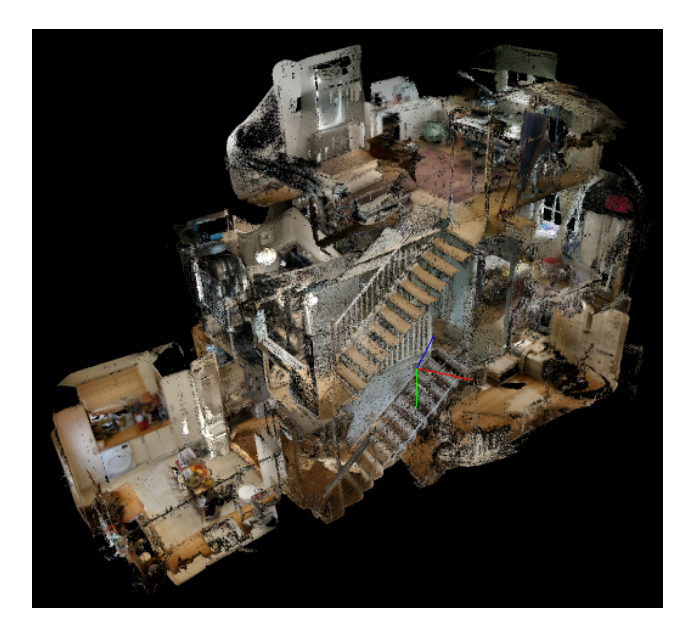


Figure 1: A globally consistent collaborative reconstruction of a three-storey house, as produced by our approach. The reconstruction involved relocalising 6 separate sequences from the *Priory* subset of our dataset.

pensating for tracking drift [17, 46, 47, 24, 14]. However, even with the most sophisticated voxel-based approaches [24, 14], capturing the data needed to reconstruct a large scene (e.g. a whole building) can take significant time and planning, and require considerable concentration on the part of the user. Moreover, the risk of transient changes to the scene (e.g. people moving around) goes up as the capture time increases, corrupting the model and forcing the user to restart the capture. There are thus good reasons to want to split the capture into several shorter sequences, which can be captured either over multiple sessions or in parallel (by multiple users) and then joined to make the whole scene.

Achieving this has traditionally been difficult: joining the sub-scenes requires the ability to accurately determine the relative transformations between them (the camera relo-

^{*}S. Golodetz, T. Cavallari and N. Lord assert joint first authorship.







Figure 2: More examples of our approach, showing the *Flat*, *House* and *Lab* subsets of our dataset.

calisation problem), even though the areas in which they overlap may never have been viewed from the same angles, and tracking drift in each sub-scene can prevent them from being joined to make a consistent overall scene. Recent advances in mobile hardware, however, such as the introduction of augmented reality smartphones that estimate their pose using visual-inertial odometry, have significantly improved our ability to capture medium-sized subscenes with little to no drift. Moreover, in RGB-D relocalisation, keyframe-based relocalisers such as random ferns [20], which were previously widely used for relocalisation in a single-user context but were unable to relocalise from novel poses, have recently been giving way to high-quality regression-based methods such as SCoRe forests [43, 45], driven by recent work [2] that showed how they could be trained and used online. Unlike keyframe-based methods, such approaches have been shown to be much better suited to relocalisation from novel poses, which is critical when aligning sub-scenes captured from different angles.

In this paper, we leverage these advances to present what to our knowledge is the first system to allow multiple users to collaborate interactively to reconstruct dense, voxel-based models of whole buildings. Unlike previous multi-agent mapping approaches, our approach is able to reconstruct detailed, globally consistent dense models. Using our system, an entire house or lab can be captured and reconstructed in under half an hour using only consumergrade hardware (see §4.5). We have integrated our approach into the open-source SemanticPaint framework [22, 21], making it easy for existing SemanticPaint and InfiniTAM [37] users to benefit from our work, and constructed a new dataset of sub-scenes to validate our approach, and we make both our code and this dataset available online. Figures 1 and 2 show reconstructions produced by our approach.

2. Related Work

Although previous work on multi-agent mapping has not focused on dense reconstruction, multi-agent mapping itself has a rich research history in computer vision and robotics, and several good surveys exist [40, 41]. Existing

approaches can be divided into two main categories:

(i) Decentralised approaches eschew the use of a central server and instead produce a local map of the scene on each agent, often transmitting these local maps between agents when they meet to share knowledge of parts of the scene that individual agents have not yet visited. For example, Cunningham et al. [12] proposed an approach called DDF-SAM, in which each robot produces a landmark-based map and shares compressed, timestamped versions of it with neighbouring robots. This was extended by [13], which registered landmark-based maps together using an approach based on Delaunay triangulation and RANSAC. The same lab later proposed DDF-SAM 2.0 [11], which avoids repeated and expensive recreation of the combined neighbourhood map through the use of 'anti-factors'. Cieslewski et al. [8] presented a sophisticated decentralised collaborative mapping back-end based on distributed version control. Choudhary et al. [6] described an approach that performs decentralised mapping using object-based maps, decreasing the bandwidth required for map sharing, but depending on the existence of pre-trained objects in the scene. Most recently, Cieslewski et al. [7] aimed to minimise the bandwidth each robot uses for inter-agent relocalisation by first establishing which other robots have relevant information, and then only communicating with the best robot found. Decentralised approaches have numerous applications, including search and rescue [30], agricultural robotics [4], planetary exploration [1] and underwater mapping [35, 44], but because of the limited computing power that tends to be available on mobile agents, most existing approaches target robustness to unreliable network connections and mechanical failures, rather than reconstructing detailed scene geometry, limiting their usefulness for tasks like building information modelling or cultural heritage preservation.

(ii) *Centralised* approaches, by contrast, can take advantage of the computing power provided by one or more central servers and their ability to communicate with all agents at once to produce detailed, globally consistent maps. For example, Chebrolu et al. [3] described a semi-dense approach based on LSD-SLAM [15] in which monocular

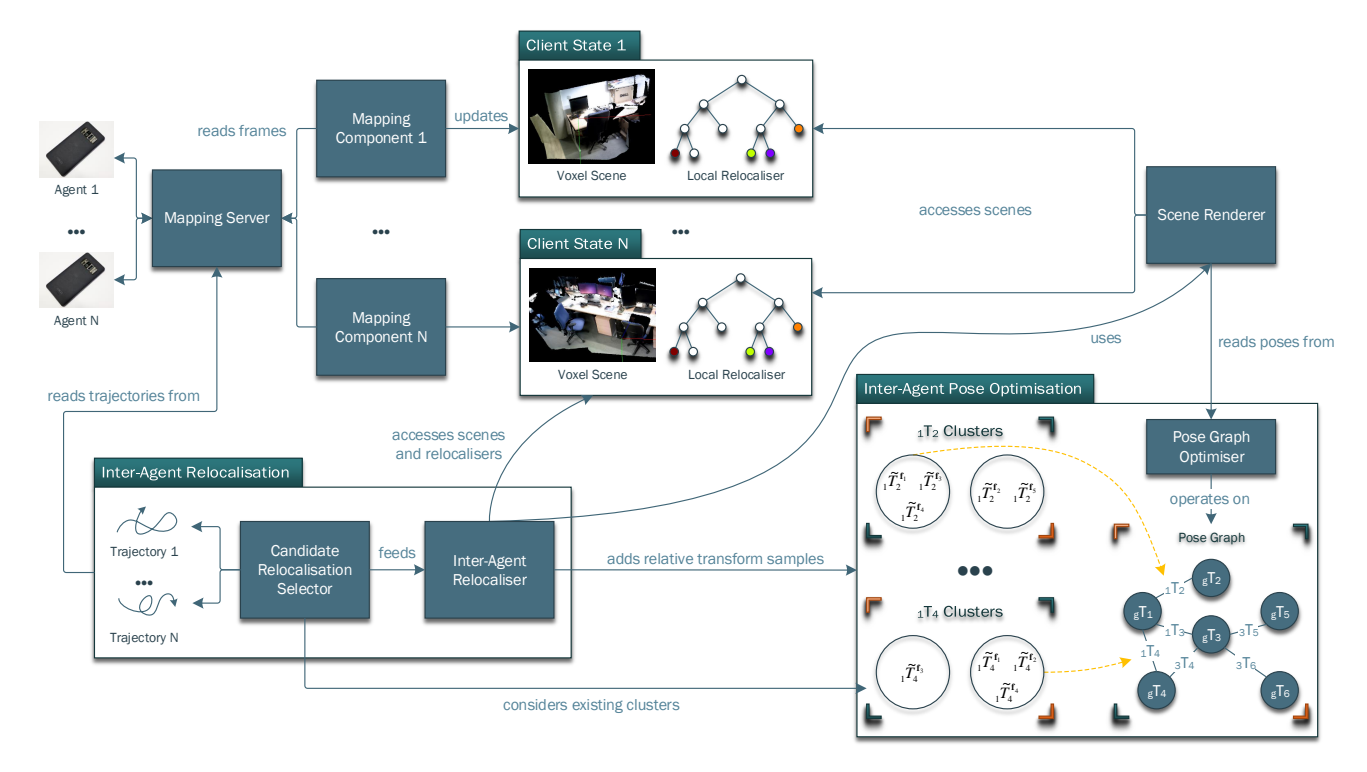


Figure 3: The architecture of our system. Individual agents (whether local or remote) track their poses and feed posed RGB-D frames to the mapping server. A separate mapping component is instantiated for each agent, which reconstructs a voxel scene and trains a local relocaliser. Separately, the candidate relocalisation selector repeatedly selects a pose from one of the agents' trajectories for relocalisation against another scene. The inter-agent relocaliser uses the scene renderer to render synthetic RGB and depth images of the corresponding scene from the selected pose, and passes them to the local relocaliser of the target scene. If a relocalisation succeeds (and is verified, see §3.3.1), a sample of the relative transform between the two scenes is recorded. The relative transform samples for each scene pair are clustered for robustness (see §3.3.2). Whenever the cluster to which a sample is added is sufficiently large, we construct a pose graph by blending the relative poses in the largest clusters, and trigger a pose graph optimisation. The optimised poses are then used for rendering the overall scene.

clients produced pose-graph maps of keyframes that were sent to a central server for optimisation. Riazuelo et al. [39] described a cloud-based distributed visual SLAM system inspired by PTAM [26]. Their clients performed tracking only, with the more expensive mapping steps being performed in the cloud. Mohanarajah et al. [31] described another cloud-based approach based on the authors' Rapyuta robotics platform. The client robots estimated their local poses by running dense, keyframe-based visual odometry on RGB-D images from a PrimeSense camera. The keyframes were then centrally optimised using g²o [27]. Forster et al. [19] demonstrated centralised, keyframe-based collaborative mapping from micro aerial vehicles (MAVs), each equipped with a monocular camera and an IMU. More recently, Schmuck and Chli [42] have shown how to incorporate server-to-client feedback into a multi-UAV collaborative approach, allowing agents to share information.

A few approaches do not fit cleanly into either category. Reid et al. [38] described a distributed approach in which multiple autonomous ground robots were controlled from a centralised ground control station (GCS), but were able to operate independently for a while if the connection to the GCS failed. McDonald et al. [29] described a stereo approach in which a single agent reconstructed a scene over multiple sessions, effectively collaborating with itself over time. Chen et al. [5] described an approach that is initially peer-to-peer, with each robot building a pose graph independently, storing its sensor data, and exchanging information with other robots on rendezvous, but later client-server, with the robots transferring their pose graphs and sensor data to a central server for pose graph optimisation and the building of a coloured point cloud map. Fankhauser et al. [16] described an approach that allowed an Asctec Firefly hexacopter and a quadrupedal ground robot to work together to help the ground robot to navigate safely. Whilst no fixedposition central server was used, the ground robot had significant computing power and effectively played the role of a server, performing bundle adjustment on data received from the hexacopter to maintain a globally consistent map.

3. Our Approach

Since we target scenarios such as building information modelling, where hardware failure is a minor concern, we adopt a centralised approach with a number of lightweight mobile clients and a powerful central server (e.g. a laptop or desktop with one or more high-end GPUs): see Figure 3. Each client estimates *accurate* local poses for a sequence of RGB-D frames (see §3.1) and transmits both the frames and the poses to the central server (see §3.2). The server constructs a sub-scene and trains a relocaliser for each client, and relocalises the sub-scenes from different clients against each other to establish a consistent global map (see §3.3).

Our system can run in either *interactive* or *batch* mode. In batch mode, all of the sub-scenes are sent across to the server (or simply read directly from disk) before any relocalisation is performed. In interactive mode, the server will start relocalising clients against each other immediately, and new clients can join on the fly to contribute to the map.

3.1. Local Tracking (Client-Side)

As mentioned above, each client in our system must estimate accurate local poses for a sequence of RGB-D frames and then transmit both the frames and the poses to the central server. This is non-trivial, since traditional pose estimation approaches, particularly those based purely on visual tracking, have tended to be subject to significant tracking drift, particularly at larger scales. For collaborative mapping, a common solution has been for clients to simply transmit inaccurate local poses and rely on the server to perform global optimisation (e.g. pose graph optimisation between keyframes [38, 5, 31] or bundle adjustment [3, 18, 42]) to achieve a globally consistent map (the optimised poses can then be sent back to the clients if desired [3, 31, 42]). However, (i) such global optimisations do not scale well, limiting the overall size of map that can be constructed, and (ii) the local poses on the clients are only corrected as global optimisations on the server finish, meaning that for much of the time they cannot be fully trusted.

In our system, we instead leverage recent developments in consumer-grade augmented reality hardware to place the burden of accurate local pose estimation on the *clients*, freeing the server to focus on reconstructing a dense global map in real time. In particular, we use a straightforward client that captures the RGB-D images and poses provided by the hardware (based on visual-inertial odometry) and transmits them to the server (see §3.2). This important choice allows us to significantly simplify the design of the server (see §3.3) and reduce server-side memory consumption, making it possible to support more agents and larger global maps.

3.2. RGB-D Frame Transmission (Client \rightarrow Server)

We use TCP between each client and the server to guarantee in-order delivery of RGB-D frames. To minimise the

network bandwidth clients use, we only transmit frames that were tracked successfully, and we compress the depth images in PNG format (lossless) and the RGB images in JPG format (lossy). Moreover, to maintain a smooth, interactive user experience on the client, we transmit messages containing the frames (and their accompanying poses) to the server on a separate thread, which iteratively reads a frame message from a *pooled queue* of reusable messages, compresses it and sends it to the server. The main thread writes uncompressed frame messages into this queue based on the current input. We discard messages that would overflow the queue (e.g. when the network is too slow to keep up with the client) to maintain interactivity and bound client memory usage; the way in which this interacts with our compression strategy is evaluated in the supplementary material.

At the server end, each client has a handler (running on a separate thread) that maintains a pooled queue of uncompressed frame messages. When a compressed frame message arrives, it is immediately uncompressed and pushed onto the queue (as on the client, we discard messages that would overflow the queue). On the main thread, we run a mapping component for each client (see §3.3), which reads RGB-D frames and their accompanying poses from its client's queue as necessary and creates a local map.

3.3. Global Mapping (Server-Side)

The server has two jobs: (i) constructing a sub-scene and training a relocaliser for each client, and (ii) determining the relative transforms between these sub-scenes to establish a global coordinate system. To achieve the first, a separate mapping component for each client (i) runs the opensource InfiniTAM reconstruction engine [36, 37] on incoming (posed) RGB-D frames to construct a voxel-based map, and (ii) trains a regression forest-based relocaliser for the sub-scene online as per Cavallari et al. [2]. To achieve the second, the server attempts to relocalise synthetic images of one agent's sub-scene using another agent's relocaliser to find estimates of the relative transform between the subscenes (see §3.3.1). These samples are clustered in transformation space to help suppress outliers, and a pose graph is constructed and optimised in the background to further refine the relative transforms between the sub-scenes (see §3.3.2). This optimisation is inspired by the single-agent sub-mapping approach of Kähler et al. [24], which showed how to build globally consistent voxel-based models by dividing a scene into small sub-scenes and optimising the relative poses between them. However, we construct a pose graph where each agent is represented by a single node, and the edges denote the relative transforms between different agents' sub-scenes. This differs from [24], where all sub-scenes came from one agent and no relocalisation was

¹Further details about the design of the pooled queue data structure can be found in the supplementary material.

needed to establish the transforms between them.

3.3.1 Inter-Agent Relocalisation

To maintain a smooth, interactive experience on the server, we attempt relocalisations between the sub-scenes of different clients on a separate thread and (if available) a separate GPU. The way in which relocalisation attempts are scheduled depends on the mode in which the server is running. In *batch* mode, relocalisations are attempted only once all of the client sub-scenes have been fully created, at which point they are attempted as quickly as possible (i.e. a new relocalisation attempt is scheduled as soon as the previous attempt finishes). In *interactive* mode, we relocalise whilst the client sub-scenes are still being reconstructed, but at most once every 20 frames: this is because relocalisers cannot be trained online and used simultaneously, so there is a need to space out relocalisation attempts to allow sufficient time in between attempts for the relocalisers to be trained.

To schedule an attempt, we first randomly generate a list of 10 candidate relocalisations. Each candidate $\mathbf{k}=(a,\mathbf{f})$, where $\mathbf{f}=(b,i)$, denotes an attempt to relocalise frame i of scene b in scene a's coordinate system. To balance different pairs of scenes, which may have been reconstructed from varying numbers of frames, we first uniformly sample an (a,b) scene pair from the set of all scene pairs, and then uniformly sample a frame index i from scene b. Each generated candidate $\mathbf{k}=(a,(b,i))$ is then scored via

$$\Phi(\mathbf{k}) = \phi_{new}(\mathbf{k}) - \phi_{conf}(\mathbf{k}) - \phi_{homog}(\mathbf{k}). \tag{1}$$

In this, ϕ_{new} aims to give a boost to candidates that might connect new nodes to the pose graph, defined as 1 if one of the sub-scenes a and b already has an optimised global pose and the other does not, and 0 otherwise. ϕ_{conf} penalises candidates that can only add a relative transform sample between a pair of sub-scenes that are already confidently relocalised with respect to each other:

$$\phi_{conf}(a,(b,i)) = \max\left(0, \max_{c \in clusters(a,b)} (|c| - N)\right). \tag{2}$$

Here, N=2 is an empirically-chosen threshold on the number of relocalisations needed before we become confident that the relative transform between a pair of sub-scenes is correct. ϕ_{homog} penalises candidates whose frame i has a local pose in scene b that is too close to (within 5cm / 5° of) one that has already been tried against scene a; we use a penalty of 5 for poses that are too close, and 0 otherwise.

Having scored the candidates, we schedule a relocalisation attempt for a candidate $\mathbf{k}=(a,\mathbf{f})$ with maximum score, where $\mathbf{f}=(b,i)$. This will proceed as shown in Figure 4. Let ${}_{\mathbf{f}}\tilde{T}_s$ denote the pose of frame \mathbf{f} in the coordinate system of a sub-scene s. First, we render synthetic RGB and depth raycasts of sub-scene b from the known pose ${}_{\mathbf{f}}\tilde{T}_b$, which we will call $\tilde{C}_b^{\mathbf{f}}$ and $\tilde{D}_b^{\mathbf{f}}$. Then, we try to relocalise

them using sub-scene a's relocaliser to obtain an estimated pose ${}_{\mathbf{f}}\tilde{T}_a$ for ${}_{\mathbf{f}}$ in a's coordinate system. To verify this estimated pose, we first render a synthetic depth raycast $\tilde{D}_a^{\mathbf{f}}$ of sub-scene a from ${}_{\mathbf{f}}\tilde{T}_a$, and compute a masked absolute depth difference image ΔD between $\tilde{D}_a^{\mathbf{f}}$ and $\tilde{D}_b^{\mathbf{f}}$ via

$$\Delta D(\mathbf{x}) = \begin{cases} \left| \tilde{D}_a^{\mathbf{f}}(\mathbf{x}) - \tilde{D}_b^{\mathbf{f}}(\mathbf{x}) \right| & \text{if } \tilde{D}_a^{\mathbf{f}}(\mathbf{x}) > 0 \text{ and } \tilde{D}_b^{\mathbf{f}}(\mathbf{x}) > 0 \\ 0 & \text{otherwise} \end{cases}, (3)$$

where \mathbf{x} ranges over Ω , the domain of $\tilde{D}_a^\mathbf{f}$ and $\tilde{D}_b^\mathbf{f}$. We then compute $\mu = (\sum_{\mathbf{x} \in \Omega} \Delta D(\mathbf{x}))/|\Omega|$, and add a relative transform sample $_a\tilde{T}_b^\mathbf{f} = (_\mathbf{f}\tilde{T}_a)^{-1}{}_\mathbf{f}\tilde{T}_b$ between a and b iff $\mu < 5$ (corresponding to 5cm). The effectiveness of this verification step is evaluated in §4.2.

3.3.2 Inter-Agent Pose Optimisation

We incrementally cluster the relative transform samples $\{aT_h^{\mathbf{f}}\}$ we add for each pair of sub-scenes (a,b) prior to performing pose graph optimisation to suppress the effect of outliers on the final result. After adding each sample, we look to see if the cluster to which the sample has just been added now has > N samples (i.e. the sample has contributed to a confident relative transform): if so, it is worthwhile to run pose graph optimisation, since the pose graph we construct may have changed since the last run. To construct the pose graph, we first compute a binary relation R(a, b) between sub-scenes such that R(a, b) is true iff the largest cluster between a and b has size > N (i.e. there is a confident relative transform between a and b). Next, we compute the reflexive, transitive closure R^* of this relation, such that $R^*(a,b)$ is true iff there is a chain (possibly empty) of confident relative transforms between a and b. Finally, we denote the scene corresponding to the first agent as the primary scene, and add to the pose graph a node for each scene that is confidently connected to the primary scene by R^* . To determine the edges to add to the graph, we filter a list containing each pair of sub-scenes for pairs (i) whose largest cluster has size $\geq N$, and (ii) such that both sub-scenes are confidently connected to the primary scene. For each surviving pair of sub-scenes (a, b), we then blend the relative transform samples $\{{}_{a}\tilde{T}_{b}^{\mathbf{f}}\}$ in the largest cluster using dual quaternion blending [25] to form an overall estimate ${}_aT_b$ of the relative transform from b to a, and add an edge to the graph. By adding only one edge for each scene pair, we keep the pose graph we are optimising small, allowing the optimisation to be run repeatedly in the background to optimise the overall map.

The goal of optimising a pose graph G is to find an optimised global pose ${}_{g}\hat{T}_{a}$ for each scene a for which there is a node in G. To perform the optimisation, we use the approach of Kähler et al. [24], as implemented in the open-source InfiniTAM reconstruction engine [36, 37]. This uses

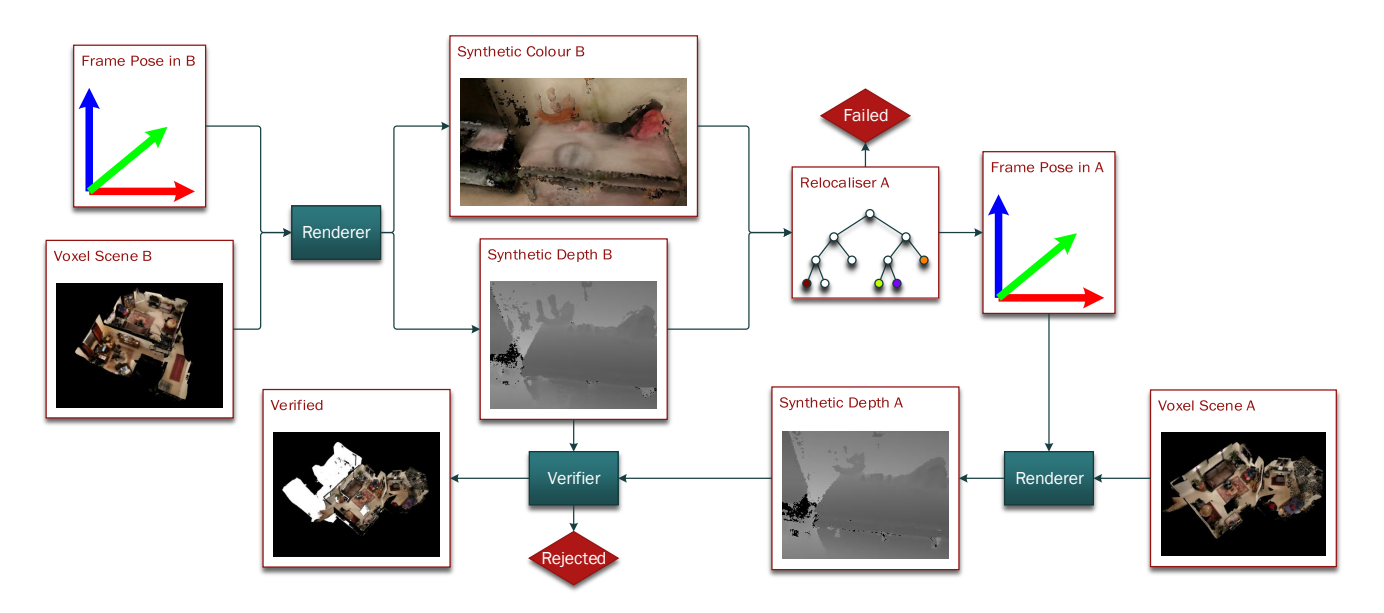


Figure 4: To relocalise the scene of an agent b against that of another agent a, we first choose an arbitrary frame from b's trajectory and render synthetic RGB and depth raycasts of b's scene from the frame's pose. Then, we try to relocalise them using a's relocaliser, which either fails, or produces an estimated pose for the frame in a's coordinate system. If a pose is proposed, we verify it by rendering a synthetic depth raycast of a's scene from the proposed pose and comparing it to the synthetic depth raycast of b's scene. We accept the pose iff the two depth raycasts are sufficiently similar (see §3.3.1).

Levenberg-Marquardt to minimise the error function

$$\epsilon(G) = \sum_{(a,b) \in edges(G)} \left\| \mathbf{v}(_g \hat{T}_b^{-1} _g \hat{T}_a _a \tilde{T}_b) \right\|_2, \tag{4}$$

where $\mathbf{v}(T) = (\hat{\mathbf{q}}(T), \mathbf{t}(T))^{\top}$ denotes the concatenation of $\hat{\mathbf{q}}(T)$, the three imaginary components of a quaternion representing the rotational part of T, and $\mathbf{t}(T)$, the translational part of T. Implicitly, this optimisation is trying to achieve ${}_g\hat{T}_a^{-1} \ {}_g\hat{T}_b = {}_a\tilde{T}_b$ for every a and b, i.e. to ensure that the optimised global poses of all the scenes are consistent with the estimated relative poses between them.

4. Experiments

We perform both quantitative and qualitative experiments to evaluate our approach. In §4.1, we evaluate the quality of a reconstruction we obtain with our collaborative approach by comparing a variety of measurements made on a combined mesh of the scene with ground-truth measurements made with a laser range finder in the real world. In §4.2, we evaluate the effectiveness of our depth difference-based verification approach (see §3.3.1), showing that our verifier is able to prune large numbers of incorrect relative transforms between the sub-scenes whilst rejecting practically no correct transforms. In §4.3, we demonstrate the scalability of our approach, showing that by using synthetic images for relocalisation and discarding data from the relocalisers we use when it is no longer needed, we can support up to 11 agents on a high-end PC. In §4.4, we evaluate

our strategy of using synthetic scene raycasts for relocalisation rather than real images from the original sequences, by testing both approaches on the standard 7-Scenes relocalisation dataset of Shotton et al. [43]. Finally, in §4.5, we time how long our approach takes to produce consistent reconstructions for four different subsets of our dataset. The supplementary material contains further analysis.

4.1. Reconstruction Quality

To demonstrate our ability to achieve high-quality collaborative reconstructions, we combined 4 sequences from the Flat subset of our dataset to reconstruct a combined map of a two-bedroom flat (see Figure 5). Since a ground-truth reconstruction of the flat was not available (and we did not have access to a LIDAR scanner with which to obtain one). we validated our reconstruction by comparing a variety of measurements made on our combined map with groundtruth measurements made with a laser range finder (a Bosch Professional GLM 40) in the real world. To achieve this, we first converted the voxel-based maps of the sub-scenes produced by InfiniTAM [36, 37] into mesh-based maps using Marching Cubes [28]. We then applied the relative transforms we had estimated between the sub-scenes during the relocalisation process to these meshes to transform them into a common coordinate system. Finally, we imported the transformed meshes into MeshLab [9], and used its pointto-point measurement tool to make our measurements. As shown in Figure 5, we found that the measurements on our

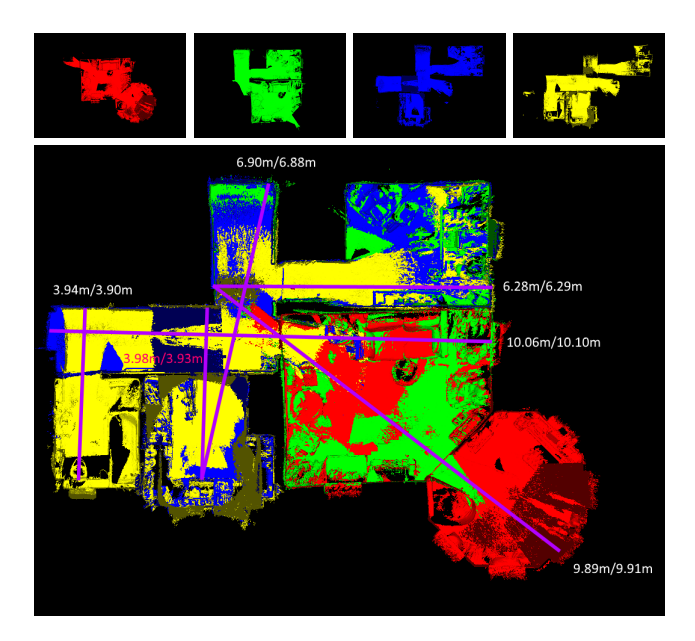


Figure 5: An example of the high-quality reconstructions we can achieve using our collaborative approach. We joined the 4 Flat sequences from our dataset to make a combined map of a two-bedroom flat. The purple lines show the measurements we performed both using a laser range finder and on a combined mesh of our model to validate our approach (the ordering of the numbers is range finder then mesh).

reconstructed model were consistently within 5cm of the ground truth, indicating that we are able to achieve reconstructions that correspond relatively well to real-world geometry. Further examples, this time showing collaborative reconstructions of multi-storey houses and a large research lab, can be found in the supplementary material.

4.2. Effectiveness of Depth Difference Verification

As mentioned in §3.3.1, we verify each proposed interagent relocalisation of a sub-scene b against a sub-scene aby rendering a synthetic depth image of scene a from the proposed pose and comparing it to the synthetic depth image from scene b that was passed to the relocaliser, masking out pixels that do not have a valid depth in both images. To evaluate the effectiveness of this approach, we first took 8 pairs of sequences $\{a, b\}$ from our dataset that we were able to successfully relocalise with respect to each other during the normal operation of our approach, and recorded the relative transform between them as the 'ground truth' transform for later use. We then attempted to relocalise every frame from scene b using the relocaliser of scene a, and vice-versa. Next, for each frame for which the relocaliser proposed a relative transform, we ran our verification step on the proposed transform, thereby classifying it as either Verified or *Rejected.* We then compared the proposed transform to the 'ground truth' transform, classifying it as Correct if it was



Figure 6: The GPU memory we use during a collaborative reconstruction of the 6 Priory sequences from our dataset.

within 5° and 5cm of the ground truth, and as *Incorrect* otherwise. Finally, we counted Verified/Correct transforms as true positives (TP), Verified/Incorrect transforms as false positives (FP), and similarly for the true negatives (TN) and false negatives (FN), as shown in Table 1.

Our results show that our verifier has an extremely high average recall rate (99.2%), meaning that it largely manages to avoid rejecting correct transforms. It also has a reasonably good average specificity (75.9%), meaning that it is fairly good at pruning the number of incorrect transforms we need to deal with. However, a fairly large number of incorrect transforms still manage to pass the verification stage: as mentioned in §3.3.2, these are dealt with later by clustering the transforms and only making use of the transforms from the largest cluster. The additional effects of this clustering step are shown in the supplementary material.

4.3. Scalability (Batch Mode)

To evaluate the scalability of our approach, we perform separate experiments for the *batch* and *interactive* modes of our system, since they target slightly different applications. The interactive experiment is in the supplementary material.

Our batch mode experiment focuses on the server's GPU memory usage as the number of agents increases. To evaluate this, we performed a collaborative reconstruction of the 6 Priory sequences from our dataset (these represent a threestory house: see the supplementary material). To maximise the number of agents we were able to handle, we added new sub-scenes to the server one at a time and deleted the training data used by each sub-scene's relocaliser once it had been fully trained: this limited the maximum memory used by the relocalisers, leaving us bounded primarily by the size of the reconstructed voxel scenes. Figure 6 shows that the final GPU memory we use for each forest-based relocaliser [2] is < 500MB, meaning that we can potentially handle around 24 relocalisers on a 12GB GPU such as an NVIDIA Titan X (the actual number may be slightly less than this due to driver overhead). Moreover, since the relocalisers we use have the same structure for each scene [2], they could potentially be merged to produce a global relocaliser and reduce memory usage still further. The memory used by the voxel scenes is currently the bottleneck preventing the scal-

Scene 1	Scene 2	Total Frames	Relocalised Frames	Verifier Performance						
				TP	FP	TN	FN	Precision	Recall	Specificity
f/bathroom2study	f/kitchen2study	4901	2190	517	931	741	1	35.7%	99.8%	44.3%
f/bathroom2study	f/study2sittingroom	4989	519	24	59	436	0	28.9%	100.0%	88.1%
f/kitchen2study	f/study2sittingroom	5544	1254	325	317	609	3	50.6%	99.1%	65.8%
f/study2sittingroom	f/turret2sittingroom	5895	1350	555	211	579	5	72.5%	99.1%	73.3%
h/frontroom2study	h/hall2frontbedroom	7714	1229	245	90	894	0	73.1%	100.0%	90.9%
h/frontroom2study	h/hall2oldkitchen	8171	1307	373	175	757	2	68.1%	99.5%	81.2%
h/hall2frontbedroom	h/hall2oldkitchen	7141	653	95	106	451	1	47.3%	99.0%	81.0%
h/hall2frontbedroom	h/mainbedroom2studio	6942	839	90	131	615	3	40.7%	96.8%	82.4%
Average (all scene pairs)		_	-	-	-	-	-	52.1%	99.2%	75.9%

Table 1: Evaluating the effectiveness of the depth difference verification we perform on proposed relocalisations between pairs of sub-scenes (see §4.2). We attempt to relocalise every frame of each sub-scene against the other using [2], and record the number of frames that we were able to relocalise, together with statistics on how many correct/incorrect relocalisations were verified/rejected by the verifier.

ing of our approach to more agents: currently, each scene takes up just over 1GB of memory, limiting us to around 11 agents on a Titan X (assuming the relocalisers are stored on a secondary GPU). To scale further, we could reduce the memory used by meshing each scene with Marching Cubes [28] and discarding the voxel maps.

4.4. Relocalisation from Synthetic Images

As per §3.3.1, we relocalise the scenes of different agents against each other using synthetic images, rather than the real RGB-D frames originally captured by the agents. This avoids the prohibitive memory cost of storing all RGB-D frames acquired by each agent in RAM (easily hundreds of MBs per agent). However, we might expect using synthetic images to lower relocalisation performance, since we train the relocalisers for each scene using the real input frames.

To verify that this is not a problem, we compared the results we are able to obtain using synthetic images to results obtained using the approach of Cavallari et al. [2] with real images on the standard 7-Scenes dataset [43]. Unlike [2], who used at most 10 modes in each leaf of their regression forests, we used at most 50 modes, since we found that this gave better results (in both cases). To test our synthetic approach, we first reconstructed each 7-Scenes sequence from the real training images as normal, then rendered synthetic frames from the testing poses, rather than using the testing images in the dataset. As Table 2 shows, our results using synthetic images were at least as good as, and in most cases actually higher than, the results using the real images, verifying that using synthetic images does not decrease relocalisation performance in practice. This is likely due to the fact that by rendering synthetic images from the reconstructed scene, we implicitly remove noise from the frames to be relocalised, improving pose estimation accuracy.

4.5. Timings

To evaluate how long it takes to produce consistent reconstructions using our approach, we computed the aver-

Sequence	Real Images	Synthetic Images		
Chess	99.85%	100.00%		
Fire	99.20%	98.85%		
Heads	100.00%	100.00%		
Office	99.80%	99.95%		
Pumpkin	90.10%	93.00%		
RedKitchen	91.34%	99.98%		
Stairs	78.30%	88.10%		

Table 2: Comparing relocalisation results obtained by rendering synthetic images of the scenes in the 7-Scenes dataset [43] from the test poses to those obtained using the real test images, by adapting a regression forest pre-trained on *Office* [2]. Percentages denote proportions of test frames with \leq 5cm translation error and \leq 5° angular error.

	Flat	Priory	House	Lab
# Sequences	4	6	4	4
Longest Sequence: # Frames	3079	1640	4372	3188
Longest Sequence: Time (s)	615.8	328.0	874.4	637.6
Average Mapping Time (s)	15.8	38.4	107.4	272.0
Average Total Time (s)	631.6	366.4	981.8	909.6

Table 3: The times taken to collaboratively reconstruct four different subsets of our dataset (see $\S4.5$).

age times taken to collaboratively reconstruct four different subsets of our dataset (see Table 3). We computed the time taken to capture the sequences in each subset as $\frac{1}{5}$ times the length of the longest sequence, assuming parallel capturing at 5Hz. The average mapping time is the time taken to relocalise the agents against each other and compute optimised global poses for their maps. To account for the random selection of frames to relocalise, we globally mapped each subset 5 times and reported the average time in the table. The average total time is from the start of the capturing process to the output of a globally consistent map: this was under half an hour for all subsets we tested.

5. Conclusion

In this paper, we have shown how to collaboratively reconstruct dense, volumetric models of 3D scenes using multiple agents. Existing collaborative mapping approaches have traditionally suffered from an inability to trust the local poses produced by their mobile agents, forcing them to perform costly global optimisations (e.g. on a server) to ensure a consistent map, and limiting their ability to perform dense, volumetric mapping collaboratively.

By leveraging recent mobile hardware advances to construct rigid local sub-scenes that do not need further refinement, and joining them using a state-of-the-art regression-based relocaliser, we avoid expensive global optimisations, opting only to refine the relative poses between individual agents' overall maps. Our system allows multiple users to collaboratively reconstruct consistent dense models of entire buildings in under half an hour using only consumergrade hardware, making it easier than ever before for users to capture detailed 3D scene models at scale.

Acknowledgements

This work was supported by Innovate UK/CCAV project #103700 (StreetWise), the EPSRC, ERC grant ERC-2012-AdG 321162-HELIOS, EPSRC grant Seebibyte EP/M013774/1 and EPSRC/MURI grant EP/N019474/1. We would also like to thank Manar Marzouk and Maria Anastasia Tsitsigkou for their help with the collaborative dataset collection.

SUPPLEMENTARY MATERIALS

A. Our Dataset

Our dataset comprises 4 different subsets – Flat, House, Priory and Lab – each containing a number of different sequences that can be successfully relocalised against each other. The name of each sequence is prefixed with a simple identifier indicating the subset to which it belongs: f/ for Flat, h/ for House, p/ for Priory and l/ for Lab. Basic information about the sequences in each subset, their frame counts and capture times can be found in Table 4. Illustrations of the sequences and how they fit together to make the combined scenes are shown in Figures 7 to 10.

Each sequence was captured at 5Hz using an Asus Zen-Fone AR augmented reality smartphone, which produces depth images at a resolution of 224×172 , and colour images at a resolution of 1920×1080 . To improve the speed at which we were able to load sequences from disk, we resized the colour images down to 480×270 (i.e. 25% size) to produce the collaborative reconstructions we show in the paper, but we nevertheless provide both the original and resized images as part of the dataset. We also provide the calibration parameters for the depth and colour sensors, the 6D poses for both sensors at each frame, and the optimised global pose produced for each sequence when running our approach on all of the sequences in each subset. Finally, we provide a pre-built mesh of each sequence, pre-transformed by its optimised global pose to allow the sequences from each subset to be loaded into MeshLab [9] or CloudCompare [10] with a common coordinate system.

B. Additional Experiments

In this section, we describe some additional experiments that we performed to evaluate our method. In §B.1, we evaluate the extent to which our approach of incrementally clustering the relative transform samples between different pairs of sub-scenes is able to remove outliers and find consistent relocalisations between the sub-scenes. In §B.2, we evaluate the scalability of our approach for interactive collaborative reconstruction. Finally, in §B.3, we evaluate the impact of frame compression on the final reconstruction quality we are able to achieve on the server. We show that with compression enabled, we can maintain real-time mapping whilst discarding fewer frames, allowing us to reconstruct higher-quality models.

Sequence	Frame Count	Capture Time (s)	
f/bathroom2study	2173	434.6	
f/kitchen2study	2728	545.6	
f/study2sittingroom	2816	563.2	
f/turret2sittingroom	3079	615.8	
h/frontroom2study	4372	874.4	
h/hall2frontbedroom	3342	668.4	
h/hall2oldkitchen	3798	759.6	
h/mainbedroom2studio	3600	720.0	
p/bath2office	1319	263.8	
p/bed2office	1518	303.6	
p/dining2guest	1232	246.4	
p/guest2bath	1315	263.0	
p/kitchen2dining	1142	228.4	
p/living2dining	1640	328.0	
1/atrium	1709	341.8	
l/firstfloor	3188	637.6	
l/groundfloor	1985	397.0	
l/secondfloor	2146	429.2	

Table 4: The sequences in each subset of our dataset.

B.1. Effectiveness of Relative Transform Clustering

As described in §3.3.2 of the main paper, we incrementally cluster the relative transform samples $\{a\tilde{T}_b^f\}$ we add for each pair of sub-scenes (a,b) prior to performing pose graph optimisation to suppress the effect of outliers on the final result. This is achieved by checking each new relative transform sample to see if there is an existing cluster to which it can be added (we specify that this is possible iff it is within 20° and $10\mathrm{cm}$ of any existing relative transform in the cluster). If so, we add the sample to the first such cluster we find; if not, we create a new cluster for it.

To evaluate the effectiveness of this approach, we took the same 8 pairs of sequences $\{a, b\}$ we used to evaluate our depth difference verifier in §4.2 of the main paper, and again relocalised every frame from scene b using the relocaliser of scene a, and vice-versa. We then counted the number of relative transform samples that were added during this process, and examined the clusters into which they had been collected. In particular, we compared the size of the largest cluster in each case (i.e. the largest 'correct' cluster) with the size of the largest cluster whose blended transform (obtained by blending all of the relative transforms in the cluster using dual quaternion blending [25]) was not within 20° and 10cm of the blended transform of the correct cluster. We refer to this latter cluster as the largest 'incorrect' cluster. The difference between these two sizes gave us a measure of the safety margin of our approach in each case, i.e.

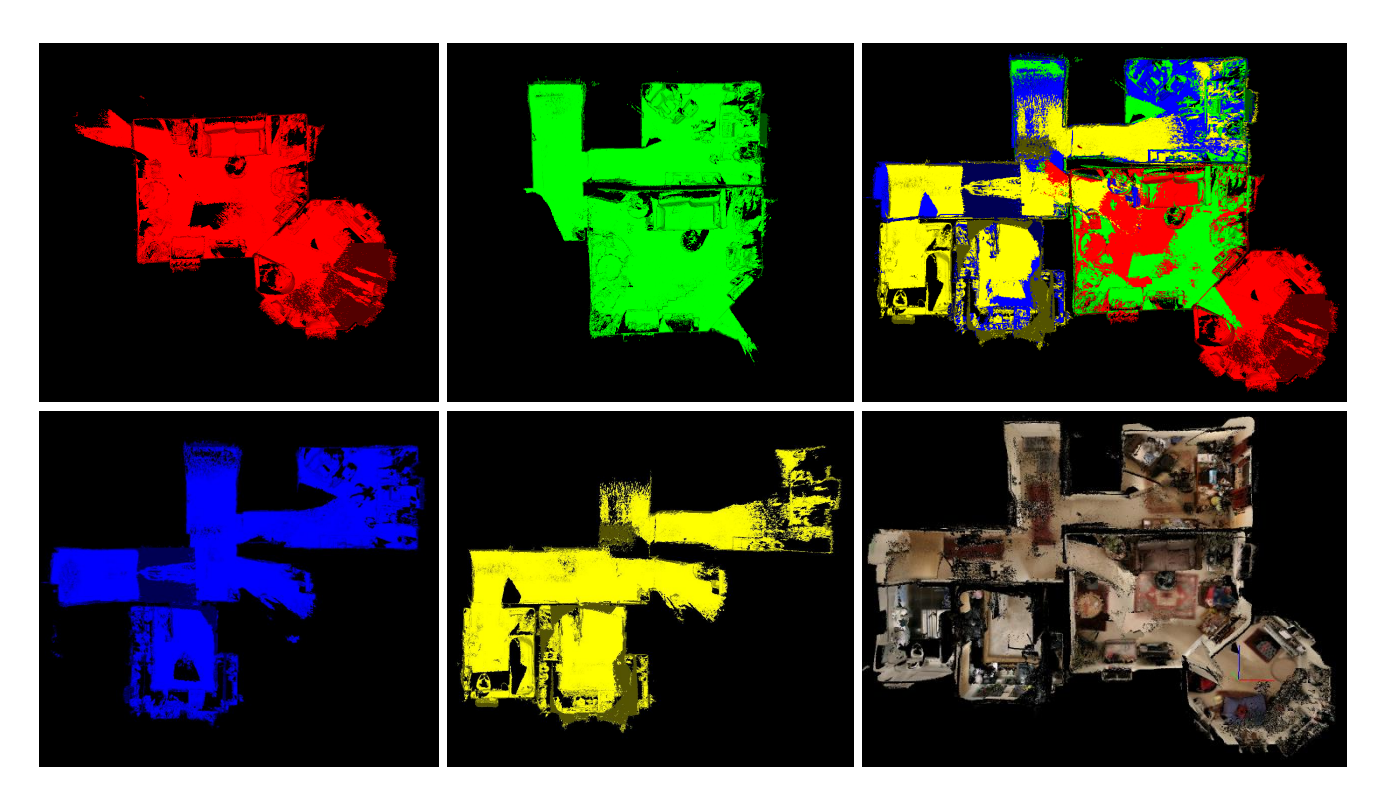


Figure 7: A collaborative reconstruction of the 4 Flat sequences in our dataset (f/turret2sittingroom, f/study2sittingroom, f/kitchen2study and f/bathroom2study). These collectively represent a single-storey, two-bedroom flat. The mono-colour images show the individual sub-scenes we reconstruct from each sequence; the other images show the combined map.

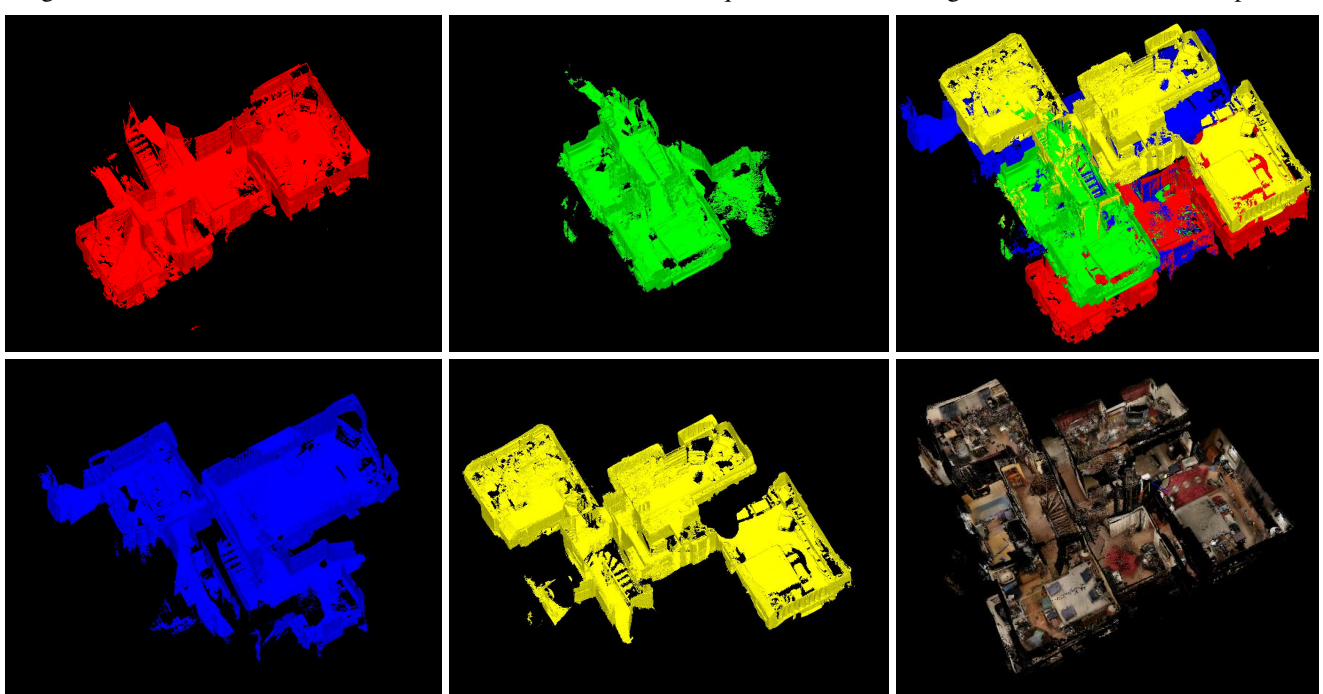


Figure 8: A collaborative reconstruction of the 4 House sequences in our dataset (h/frontroom2study, h/hall2frontbedroom, h/hall2oldkitchen and h/mainbedroom2studio). These collectively represent a two-storey, four-bedroom house. The monocolour images show the individual sub-scenes we reconstruct from each sequence; the other images show the combined map.

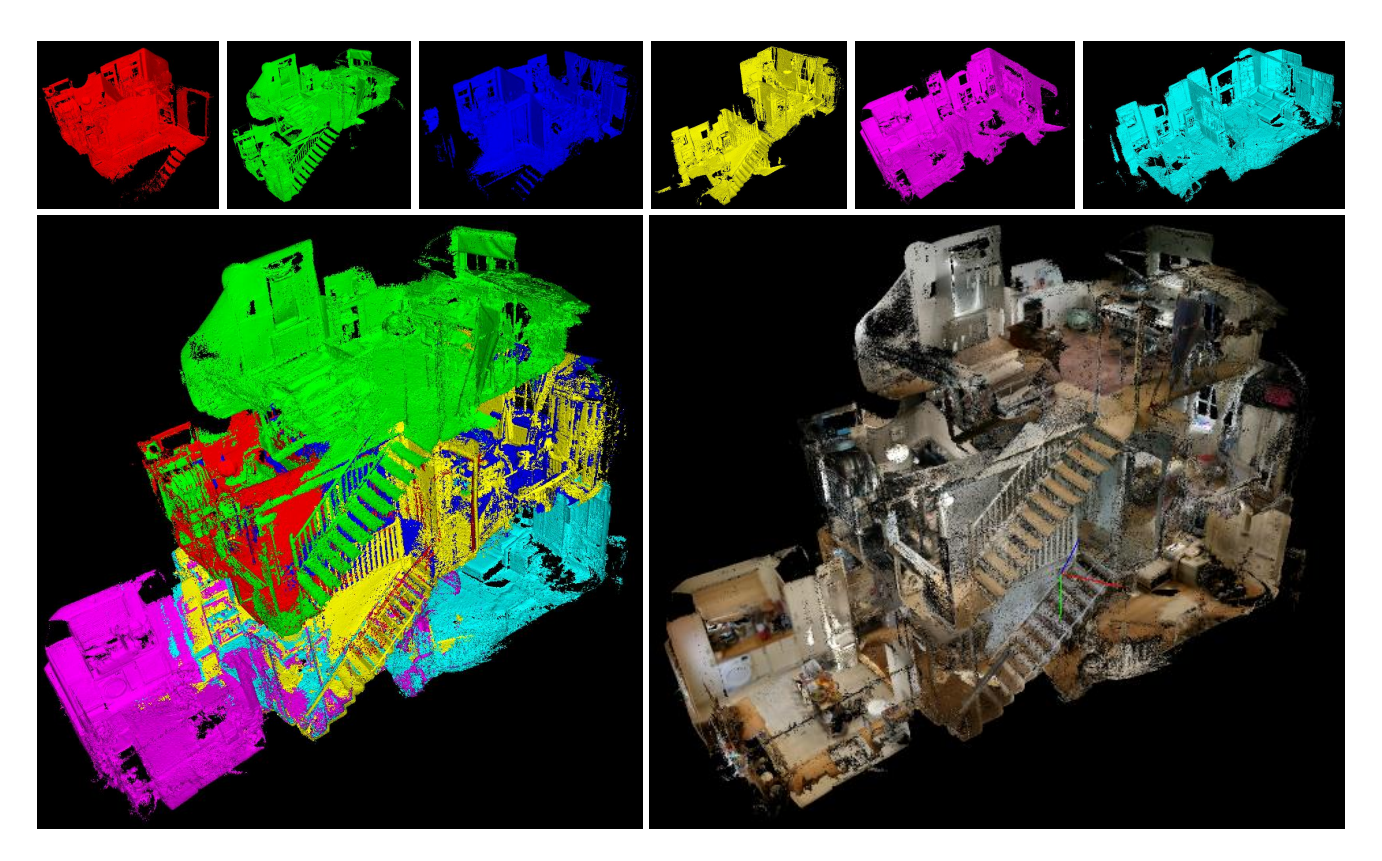


Figure 9: A collaborative reconstruction of the 6 Priory sequences in our dataset (*p/bath2office*, *p/bed2office*, *p/guest2bath*, *p/dining2guest*, *p/kitchen2dining* and *p/living2dining*). These collectively represent a three-storey house. The mono-colour images show the individual sub-scenes we reconstruct from each sequence; the other images show the combined map.

the number of consistent erroneous samples that would need to have been added to the largest incorrect cluster to cause it to have been chosen instead of the correct cluster.

As our results in Table 5 show, for most pairs of scenes the size of the correct cluster was significantly larger than the size of the largest incorrect cluster, indicating that in practice we are very likely to accumulate $\geq N$ samples from the correct cluster and become confident about it long before we accumulate > N samples from an incorrect cluster. For two pairs of scenes (f/bathroom2study & f/study2sittingroom, and h/hall2frontbedroom & h/mainbedroom2studio), the safety margins were much lower than in the other cases. However, in both cases, the pairs of scenes in question have comparatively low overlap (see the green and yellow sequences in both Figures 7 and 8). Moreover, whilst the blended transforms of the correct cluster and the largest incorrect cluster in each case were not within 20° and 10cm of each other, a manual inspection of the relevant transforms showed that they were still comparatively close (within 50° and 50cm), meaning that the safety margin before hitting a cluster with a grossly incorrect blended transform is in practice somewhat higher in each case.

B.2. Scalability (Interactive Mode)

To evaluate the scalability of our approach in *interactive* mode, we time a collaborative reconstruction involving a server and three different clients: (i) a desktop using a Kinect camera and a relocaliser based on random ferns [20], connected to the server over a wired network, (ii) a laptop using an Orbbec Astra S camera and a regression forest relocaliser [2], connected to the server over WiFi, and (iii) a local process on the same machine as the server that reads posed RGB-D frames from disk.

The frame processing times on the server and each client over the course of this experiment, together with a detailed description of what is happening at each stage during the process, are shown in Figure 11. As might be expected, the time taken per frame on each client is unaffected by the number of other agents connected to the server, allowing local reconstruction to remain interactive even when many clients are connected. Moreover, the time taken per frame on the server increases by only a small amount for each additional agent added, allowing the server user to continue to view the collaborative reconstruction interactively from different angles even when multiple different clients are connected. With a large number of clients connected, the

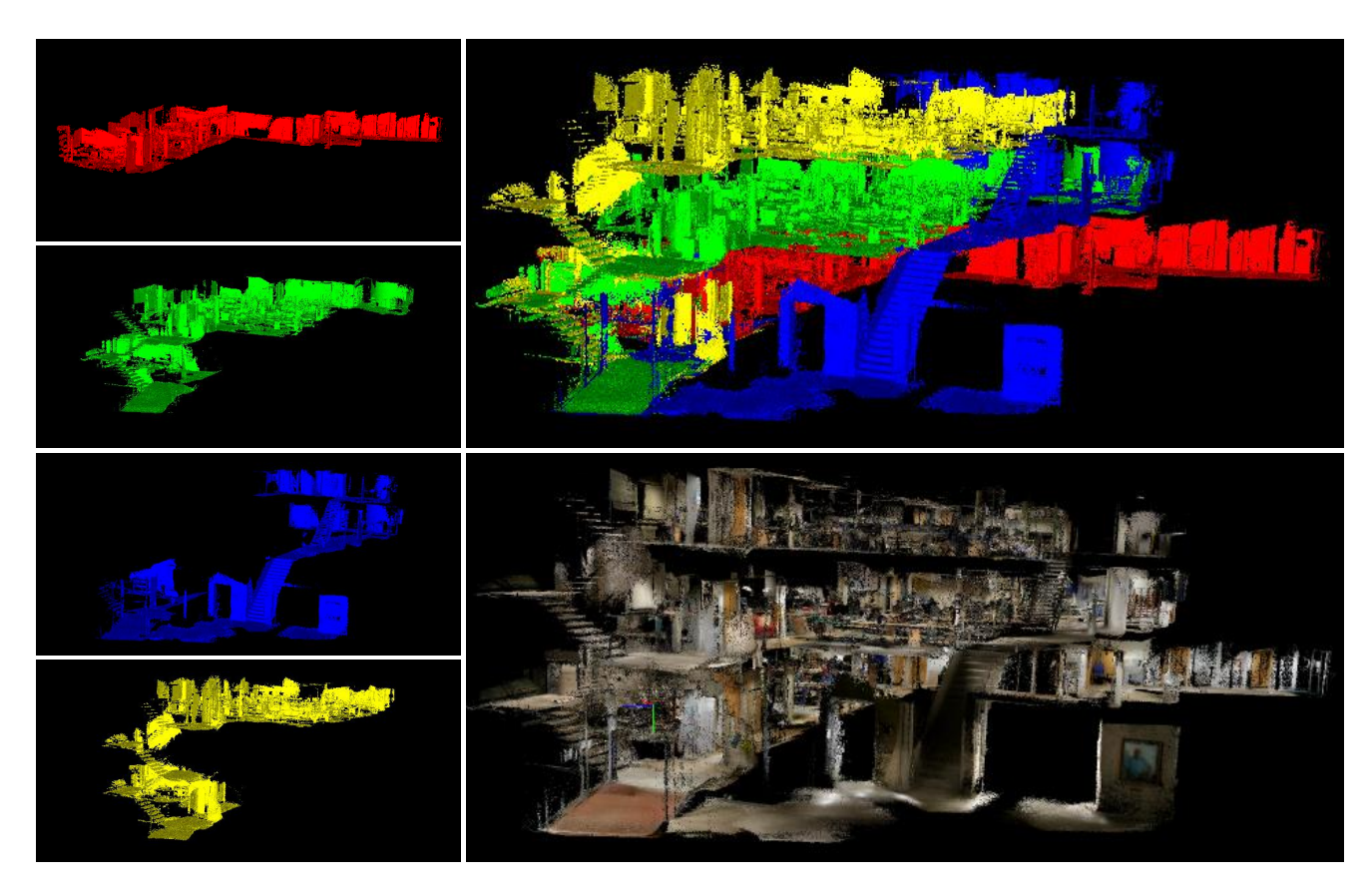


Figure 10: A collaborative reconstruction of the 4 Lab sequences in our dataset (*l/groundfloor*, *l/gristfloor*, *l/atrium* and *l/secondfloor*). These collectively represent a three-storey research lab. The mono-colour images show the individual subscenes we reconstruct from each sequence; the other images show the combined map.

Scene 1	Scene 2	Total Frames	Samples Added	Correct Cluster	Largest Incorrect Cluster	Safety Margin
f/bathroom2study	f/kitchen2study	4901	1472	1317 (89.5%)	18 (1.2%)	1299
f/bathroom2study	f/study2sittingroom	4989	82	21 (25.6%)	18 (22.0%)	3
f/kitchen2study	f/study2sittingroom	5544	589	506 (85.9%)	5 (0.8%)	501
f/study2sittingroom	f/turret2sittingroom	5895	765	759 (99.2%)	2 (0.3%)	757
h/frontroom2study	h/hall2frontbedroom	7714	360	249 (69.2%)	16 (4.4%)	233
h/frontroom2study	h/hall2oldkitchen	8171	592	442 (74.7%)	10 (1.7%)	432
h/hall2frontbedroom	h/hall2oldkitchen	7141	242	192 (79.3%)	12 (5.0%)	180
h/hall2frontbedroom	h/mainbedroom2studio	6942	260	102 (39.2%)	69 (26.5%)	33

Table 5: Evaluating the extent to which our approach of incrementally clustering the relative transform samples between different pairs of sub-scenes is able to remove outliers and find consistent relocalisations between the sub-scenes. We attempt to relocalise every frame of each sub-scene against the other using [2], and record the total number of samples that were added (equal to the number of relocalised frames that passed depth difference verification), and the sizes of the correct cluster and the largest incorrect cluster produced by our method in each case (together with the percentages of the samples added these sizes represent). The safety margin for each scene pair refers to the number of consistent erroneous samples that would need to have been added to the largest incorrect cluster to cause it to have been chosen instead of the correct cluster.

server currently becomes less interactive because the mapping components for each client are being run sequentially: this is something we plan to mitigate in the future by running all of the mapping components in parallel.

B.3. Frame Compression

To demonstrate the impact that compressing the RGB-D frames we transmit over the network has on the final reconstruction quality on the server, we used CloudCompare [10] to compare a locally-reconstructed reference model of an office with two reconstructions performed from frame

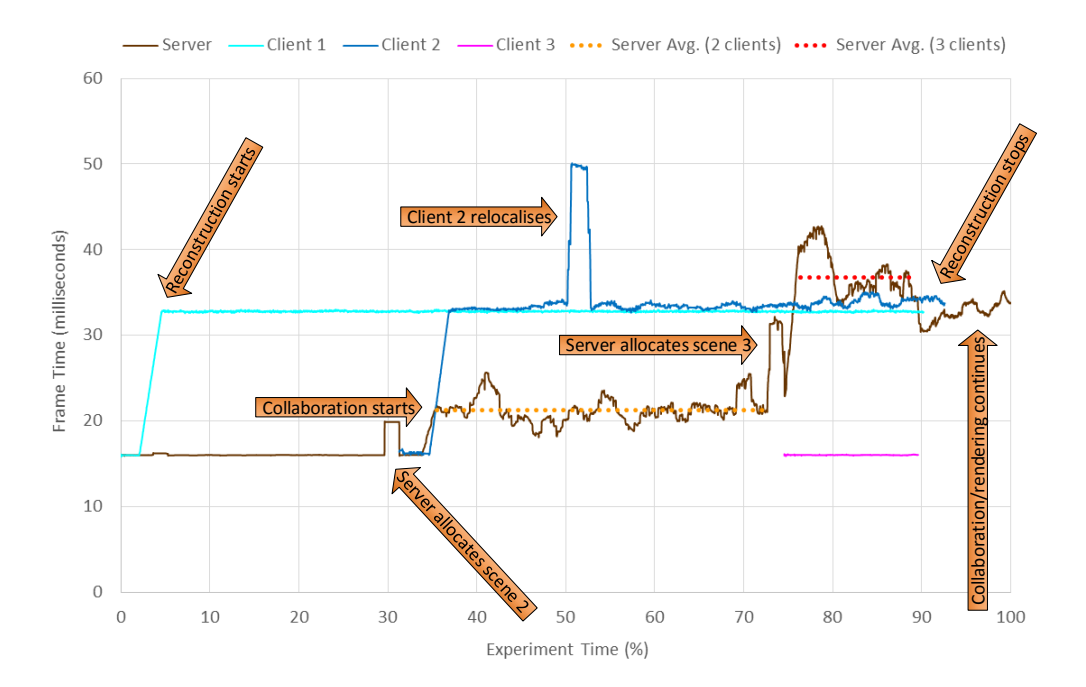


Figure 11: An experiment showing how the frame processing times on the server and each of three individual clients change over the course of a collaborative reconstruction using our system. Note that we smooth these times over a 100-frame window to make the graph slightly easier to read. Prior to the start of the experiment, the server allocates a mapping component for the first client and waits for it to connect. The experiment starts when the first client (a desktop using a Kinect camera and a relocaliser based on random ferns [20]) connects to the server over a wired network. Reconstruction begins when the client starts sending RGB-D frames to the server. Subsequently, a second client (a laptop using an Orbbec Astra S camera and a regression forest relocaliser [2]) connects to the server over WiFi. This causes the server to allocate a mapping component for the second client and start reconstructing a local scene based on the RGB-D frames that it sends across. In parallel, the server starts trying to relocalise the local scenes of the two clients against each other on a separate thread. Around half way through the experiment, the tracking on the second client fails, triggering a local relocalisation that causes a spike in processing time on the client. Towards the end of the experiment, a third client (this time a local one on the same machine as the server that reads posed RGB-D frames from disk) connects, and the server again allocates a mapping component for it. The processing time on this client is lower because it does not need to perform camera tracking. At this point, the server is trying to relocalise all three local scenes against each other. Finally, all three clients disconnect, and reconstruction stops. However, inter-agent relocalisation continues on the server until a consistent reconstruction is achieved, and the server continues rendering all three local scenes to allow the user to visualise what is happening.

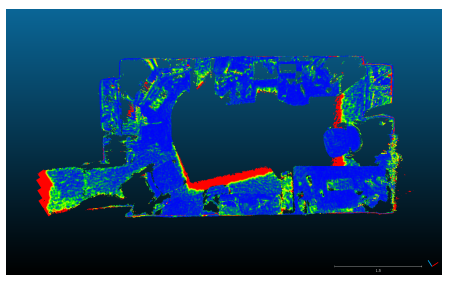
data sent over a WiFi connection, one with frame compression disabled and the other with it enabled (see Figure 12). We measured the bandwidth of this WiFi connection to be roughly 8 Mbits/s, which is less than the roughly 25 Mbits/s that we needed to transmit the same sequence in compressed form without loss over a wired connection, and much less than the roughly 250 Mbits/s that would have been needed to transmit the sequence without loss uncompressed. In other words, with compression enabled, we are able to transmit around 1 in 3 of the frames in the sequence over WiFi whilst maintaining real-time rates; without compression, this drops to more than 1 in 30. As Figure 12 shows, this has a significant effect on the resulting reconstruction quality: with compression disabled (b), we lose some parts of the map completely and have a higher error

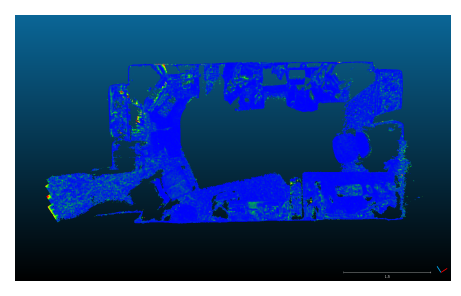
rate across the map as a whole; with compression enabled (c), we manage to reconstruct more or less the entire map, and the error rate is greatly reduced.

C. Additional Implementation Details

In this section, we describe some implementation details that might be relevant for anyone wanting to reimplement our approach, namely the inner workings of the pooled queue data structure mentioned in §3.2 of the main paper, and the way in which we can render a global map of all of the sub-scenes we have reconstructed. These details can be skipped by more casual readers.







(a) Reference Model

(b) Reference vs. Uncompressed

(c) Reference vs. Compressed

Figure 12: An example showing the impact of frame compression on the reconstruction quality we are able to achieve on the server whilst maintaining real-time frame rates by discarding some frames: (a) a locally-reconstructed reference model of an office; (b) the differences between the reference model and a model reconstructed from the frames that we managed to transmit without using compression; (c) the differences between the reference model and a model reconstructed from the frames that we managed to transmit with compression. The comparisons were made using CloudCompare [10]. The errors range from blue = 0cm to red \geq 5cm (or missing). With compression enabled, we are forced to discard far fewer frames, allowing us to achieve a much lower error rate with respect to the reference model.

C.1. Pooled Queue Data Structure

A pooled queue is a data structure that pairs a normal queue Q of objects of type T with a pool P of reusable T objects, with the underlying goal of minimising memory reallocations for performance reasons. Normal queues conventionally support the following range of operations: empty checks whether the queue is empty, peek gets the object (if any) at the front of the queue, pop removes the object (if any) at the front of the queue, push adds an object to the back of the queue, and size gets the number of objects on the queue. Pooled queues support the same range of operations, but their implementations of push and pop are necessarily complicated by interactions with the pool.

The pop operation is the more straightforward of the two: this simply removes the object (if any) at the front of the queue and returns it to the pool (with appropriate synchronisation in a multi-threaded context).

The push operation is more complicated, and we divide it into two parts: begin_push and end_push. The begin_push operation first checks whether a reusable object is currently available from the pool. If so, it removes it from the pool and returns a push handler encapsulating the object to the caller. The caller then modifies the object, after which the push handler calls end_push to actually push the object onto the queue. If a reusable object is not available from the pool when begin_push is called, we have a range of options, which are available as policies in our implementation: (i) discard the object we are trying to push onto the queue, (ii) grow the pool by allocating a new object that can then be reused, (iii) remove a random element from the queue and return it to the pool so that it can be reused, or (iv) wait for another thread to pop an object from the queue and return it to the pool. In practice, we

found the discard strategy to work best for our approach: growing the pool has the disadvantage that the memory usage can grow without bound over time, waiting makes the client and/or server (as the case may be) less interactive, and removing a random element from the queue functions much like discarding but with different frames.

C.2. Global Map Rendering

To render a global map of all of the sub-scenes we have reconstructed from a global pose $T_g \in SE_3$, we first compute (for each agent a) the corresponding local pose T_a in a's local coordinate system:

$$T_a = T_g \,_g \hat{T}_a \tag{5}$$

Using the standard raycasting approach for a voxel-based scene [37], we then render synthetic colour and depth images (at 1280×960 resolution) for each agent from the local pose we have computed for it, which we call C_a and D_a respectively. Finally, we set the colour of each pixel in the output image $\mathcal O$ based on per-pixel depth testing between the agents, i.e.

$$\mathcal{O}(\mathbf{x}) = C_{a^*}(\mathbf{x}), \text{ where } a^* = \operatorname*{argmin}_a D_a(\mathbf{x}),$$
 (6)

where x ranges over the domain of \mathcal{O} .

References

- [1] A. Bajpai, G. Burroughes, A. Shaukat, and Y. Gao. Planetary Monocular Simultaneous Localization and Mapping. *JFR*, 33(2):229–242, 2016. 2
- [2] T. Cavallari, S. Golodetz*, N. A. Lord*, J. Valentin, L. D. Stefano, and P. H. S. Torr. On-the-Fly Adaptation of Regression Forests for Online Camera Relocalisation. In CVPR, 2017. 2, 4, 7, 8, 12, 13, 14
- [3] N. Chebrolu, D. Marquez-Gamez, and P. Martinet. Collaborative Visual SLAM Framework for a Multi-Robot System. In PPNIV, 2015. 2, 4
- [4] F. A. A. Cheein and R. Carelli. Agricultural Robotics: Unmanned Robotic Service Units in Agricultural Tasks. *IEEE Industrial Electronics Magazine*, 7(3), 2013.
- [5] H. Chen, J. Zhong, Y. Fu, and Y. Lou. Pose-graph Based 3D Map Fusion with Distributed Robot System. In *ROBIO*, 2014. 3, 4
- [6] S. Choudhary, L. Carlone, C. Nieto, J. Rogers, H. I. Christensen, and F. Dellaert. Distributed Mapping with Privacy and Communication Constraints: Lightweight Algorithms and Object-based Models. arXiv preprint arXiv:1702.03435, 2017. 2
- [7] T. Cieslewski, S. Choudhary, and D. Scaramuzza. Data-Efficient Decentralized Visual SLAM. arXiv preprint arXiv:1710.05772, 2017. 2
- [8] T. Cieslewski, S. Lynen, M. Dymczyk, S. Magnenat, and R. Siegwart. Map API – Scalable Decentralized Map Building for Robots. In *ICRA*, pages 6241–6247, 2015. 2
- [9] P. Cignoni, M. Callieri, M. Corsini, M. Dellepiane, F. Ganovelli, and G. Ranzuglia. MeshLab: an Open-Source Mesh Processing Tool. In *Eurographics Italian Chapter Conference*, pages 129–136, 2008. 6, 10
- [10] CloudCompare v2.9 (GPL software), 2017. Retrieved from http://www.danielgm.net/cc. 10, 13, 15
- [11] A. Cunningham, V. Indelman, and F. Dellaert. DDF-SAM 2.0: Consistent Distributed Smoothing and Mapping. In *ICRA*, pages 5220–5227, 2013.
- [12] A. Cunningham, M. Paluri, and F. Dellaert. DDF-SAM: Fully Distributed SLAM using Constrained Factor Graphs. In *IROS*, pages 3025–3030, 2010. 2
- [13] A. Cunningham, K. M. Wurm, W. Burgard, and F. Dellaert. Fully Distributed Scalable Smoothing and Mapping with Robust Multi-robot Data Association. In *ICRA*, pages 1093– 1100, 2012. 2
- [14] A. Dai, M. Nießner, M. Zollhöfer, S. Izadi, and C. Theobalt. BundleFusion: Real-time Globally Consistent 3D Reconstruction using Online Surface Re-integration. *TOG*, 36(3):24, 2017. 1
- [15] J. Engel, T. Schöps, and D. Cremers. LSD-SLAM: Large-Scale Direct Monocular SLAM. In ECCV, pages 834–849, 2014. 2
- [16] P. Fankhauser, M. Bloesch, P. Krüsi, R. Diethelm, M. Wermelinger, T. Schneider, M. Dymczyk, M. Hutter, and R. Siegwart. Collaborative Navigation for Flying and Walking Robots. In *IROS*, pages 2859–2866, 2016. 3

- [17] N. Fioraio, J. Taylor, A. Fitzgibbon, L. D. Stefano, and S. Izadi. Large-Scale and Drift-Free Surface Reconstruction Using Online Subvolume Registration. In CVPR, pages 4475–4483, 2015. 1
- [18] P. Fleck, C. Arth, C. Pirchheim, and D. Schmalstieg. Tracking and Mapping with a Swarm of Heterogeneous Clients. In ISMAR, 2015. 4
- [19] C. Forster, S. Lynen, L. Kneip, and D. Scaramuzza. Collaborative Monocular SLAM with Multiple Micro Aerial Vehicles. In *IROS*, pages 3962–3970, 2013. 3
- [20] B. Glocker, J. Shotton, A. Criminisi, and S. Izadi. Real-Time RGB-D Camera Relocalization via Randomized Ferns for Keyframe Encoding. *TVCG*, 21(5):571–583, May 2015. 2, 12, 14
- [21] S. Golodetz*, M. Sapienza*, J. P. C. Valentin, V. Vineet, M.-M. Cheng, A. Arnab, V. A. Prisacariu, O. Kähler, C. Y. Ren, D. W. Murray, S. Izadi, and P. H. S. Torr. SemanticPaint: A Framework for the Interactive Segmentation of 3D Scenes. Technical Report TVG-2015-1, Department of Engineering Science, University of Oxford, October 2015. Released as arXiv e-print 1510.03727.
- [22] S. Golodetz*, M. Sapienza*, J. P. C. Valentin, V. Vineet, M.-M. Cheng, V. A. Prisacariu, O. Kähler, C. Y. Ren, A. Arnab, S. L. Hicks, D. W. Murray, S. Izadi, and P. H. S. Torr. SemanticPaint: Interactive Segmentation and Learning of 3D Worlds. In ACM SIGGRAPH Emerging Technologies, page 22, 2015. 2
- [23] J. Huang, A. Dai, L. Guibas, and M. Niessner. 3DLite: Towards Commodity 3D Scanning for Content Creation. *TOG*, 2017.
- [24] O. Kähler, V. A. Prisacariu, and D. W. Murray. Real-Time Large-Scale Dense 3D Reconstruction with Loop Closure. In *ECCV*, pages 500–516, 2016. 1, 4, 5
- [25] L. Kavan, S. Collins, C. O'Sullivan, and J. Zara. Dual Quaternions for Rigid Transformation Blending. Technical Report TCD-CS-2006-46, Trinity College Dublin, 2006. 5, 10
- [26] G. Klein and D. Murray. Parallel Tracking and Mapping for Small AR Workspaces. In *ISMAR*, pages 225–234, 2007. 3
- [27] R. Kümmerle, G. Grisetti, H. Strasdat, K. Konolige, and W. Burgard. g²o: A General Framework for Graph Optimization. In *ICRA*, pages 3607–3613, 2011. 3
- [28] W. E. Lorensen and H. E. Cline. Marching Cubes: A High Resolution 3D Surface Construction Algorithm. ACM SIG-GRAPH Computer Graphics, 21(4):163–169, 1987. 6, 8
- [29] J. McDonald, M. Kaess, C. Cadena, J. Neira, and J. J. Leonard. Real-time 6-DOF multi-session visual SLAM over large-scale environments. *RAS*, 61(10):1144–1158, 2013. 3
- [30] N. Michael, S. Shen, K. Mohta, Y. Mulgaonkar, V. Kumar, K. Nagatani, Y. Okada, S. Kiribayashi, K. Otake, K. Yoshida, K. Ohno, E. Takeuchi, and S. Tadokoro. Collaborative Mapping of an Earthquake-Damaged Building via Ground and Aerial Robots. *JFR*, 29(5):832–841, 2012. 2
- [31] G. Mohanarajah, V. Usenko, M. Singh, R. D'Andrea, and M. Waibel. Cloud-based Collaborative 3D Mapping in Real-Time with Low-Cost Robots. *TASE*, 12(2):423–431, 2015. 3, 4

- [32] S. Murali, P. Speciale, M. R. Oswald, and M. Pollefeys. Indoor Scan2BIM: Building Information Models of House Interiors. In *IROS*, 2017. 1
- [33] R. A. Newcombe, S. Izadi, O. Hilliges, D. Molyneaux, D. Kim, A. J. Davison, P. Kohli, J. Shotton, S. Hodges, and A. Fitzgibbon. KinectFusion: Real-Time Dense Surface Mapping and Tracking. In *ISMAR*, pages 127–136, 2011. 1
- [34] M. Nießner, M. Zollhöfer, S. Izadi, and M. Stamminger. Real-time 3D Reconstruction at Scale using Voxel Hashing. *TOG*, 32(6):169, 2013. 1
- [35] L. Paull, G. Huang, M. Seto, and J. J. Leonard. Communication-Constrained Multi-UAV Cooperative SLAM. In *ICRA*, pages 509–516, 2015.
- [36] V. A. Prisacariu, O. Kähler, M. M. Cheng, C. Y. Ren, J. Valentin, P. H. S. Torr, I. D. Reid, and D. W. Murray. A Framework for the Volumetric Integration of Depth Images. *arXiv preprint arXiv:1410.0925*, 2014. 1, 4, 5, 6
- [37] V. A. Prisacariu, O. Kähler, S. Golodetz, M. Sapienza, T. Cavallari, P. H. S. Torr, and D. W. Murray. InfiniTAM v3: A Framework for Large-Scale 3D Reconstruction with Loop Closure. *arXiv preprint arXiv:1708.00783v1*, 2017. 1, 2, 4, 5, 6, 15
- [38] R. Reid, A. Cann, C. Meiklejohn, L. Poli, A. Boeing, and T. Braunl. Cooperative Multi-Robot Navigation, Exploration, Mapping and Object Detection with ROS. In *IV*, 2013. 3, 4
- [39] L. Riazuelo, J. Civera, and J. M. M. Montiel. C²TAM: A Cloud framework for cooperative tracking and mapping. *RAS*, 62(4):401–413, 2014. 3
- [40] W. Rone and P. Ben-Tzvi. Mapping, localization and motion planning in mobile multi-robotic systems. *Robotica*, 31:1– 23, 2013. 2
- [41] S. Saeedi, M. Trentini, M. Seto, and H. Li. Multiple-robot Simultaneous Localization and Mapping – A Review. *JFR*, 33(1):3–46, 2016.
- [42] P. Schmuck and M. Chli. Multi-UAV Collaborative Monocular SLAM. In *ICRA*, pages 3863–3870, 2017. 3, 4
- [43] J. Shotton, B. Glocker, C. Zach, S. Izadi, A. Criminisi, and A. Fitzgibbon. Scene Coordinate Regression Forests for Camera Relocalization in RGB-D Images. In CVPR, pages 2930–2937, 2013. 2, 6, 8
- [44] L. Silveira, F. Guth, P. Drews-Jr, P. Ballester, M. Machado, F. Codevilla, N. Duarte-Filho, and S. Botelho. An Opensource Bio-inspired Solution to Underwater SLAM. *IFAC-PapersOnLine*, 48(2):212–217, 2015.
- [45] J. Valentin, M. Nießner, J. Shotton, A. Fitzgibbon, S. Izadi, and P. Torr. Exploiting Uncertainty in Regression Forests for Accurate Camera Relocalization. In CVPR, pages 4400– 4408, 2015. 2
- [46] T. Whelan, M. Kaess, H. Johannsson, M. Fallon, J. J. Leonard, and J. McDonald. Real-time large scale dense RGB-D SLAM with volumetric fusion. *IJRR*, 34(4-5):598– 626, 2015.
- [47] T. Whelan, S. Leutenegger, R. F. Salas-Moreno, B. Glocker, and A. J. Davison. ElasticFusion: Dense SLAM Without A Pose Graph. In *RSS*, 2015. 1

[48] M. Zollhöfer, C. Siegl, M. Vetter, B. Dreyer, M. Stamminger, S. Aybek, and F. Bauer. Low-Cost Real-Time 3D Reconstruction of Large-Scale Excavation Sites. *JOCCH*, 9(1), 2016. 1